Piston cylinder cell for high pressure ultrasonic pulse echo measurements

Piston Cylinder Cell for High Pressure Ultrasonic Pulse Echo Measurements

M. W. Kepa,[1, a)] C. J. Ridley,[2] K. V. Kamenev,[2] and A. D. Huxley[1]
[1)] *SUPA, Centre for Science at Extreme Conditions and School of Physics and Astronomy, University of Edinburgh, Edinburgh EH9 3JZ, United Kingdom*
[2)] *Centre for Science at Extreme Conditions and School of Engineering, University of Edinburgh, Edinburgh EH9 3FD, United Kingdom*

(Dated: 24 June 2016)

Ultrasonic techniques such as Pulse Echo, Vibrating Reed or Resonant Ultrasound Spectroscopy are powerful probes not only for studying elasticity but also for investigating electronic and magnetic properties. Here, we report on the design of a high pressure ultrasonic pulse echo apparatus, based on a piston cylinder cell, with a simplified electronic setup that operates with a single coaxial cable and requires sample lengths of mm only. The design allows simultaneous measurements of ultrasonic velocities and attenuation coefficients up to a pressure of 1.5 GPa. We illustrate the performance of the cell by probing the phase diagram of a single crystal of the ferromagnetic superconductor UGe_2.

Keywords: High-pressure, Ultrasonic Measurements, Low Temperature

I. INTRODUCTION

Ultrasound is a powerful probe in condensed matter physics. Not only can it provide information on the elastic tensor but it can also provide the means for detecting phase transitions (including structural, electrical and magnetic) as well as sample defects.[1,2] Piezoelectric transducers are the most popular devices for generating ultrasonic waves. In a simple setting, a single transducer is attached, by mechanical clamping or by chemical bonding, to a sample with known geometry, and it acts as an emitter and a receiver of ultrasonic pulses. This technique allows the absolute speed of sound to be measured directly.[1,2]

The pulse echo technique was applied with a Paris-Edinburgh cell[3] up to a pressure of 6 GPa, a diamond anvil cell[4] up to 10 GPa, a piston cylinder cell[5,6] up to 2 GPa and also a multi-anvil cell[7] up to 7 GPa. These experiments were performed mainly to study geological samples at high pressures and temperatures relevant to investigations of the Earth's mantle.[8] They also shared the same design whereby the transducer was positioned outside the pressure region and the ultrasonic pulses were transmitted through the anvil, piston or buffer rod depending on the type of cell. Positioning the transducer in this way requires a careful analysis of the ultrasonic spectrum to account for the contribution from these elements which add to the background signal.

The pulse echo technique was also used to study strongly correlated systems such as the heavy fermion UPt_3 whose multiple superconducting phases were probed by the ultrasonic measurements.[9,10] The material was also studied under moderate uniaxial pressure (up to 0.3 GPa) with a continuous wave ultrasonic technique, which helped to extend its phase diagram.[11] URu_2Si_2 is another example of a heavy fermion studied under hydrostatic pressure in a piston cylinder cell up to 1.6 GPa.[12]

Here, we present the development of a piston cylinder cell and pulse echo technique with the transducer installed inside the pressure space employing a simple electronic setup suitable for single crystal measurements. We present test data taken on the ferromagnetic superconductor UGe_2 which are consistent with the established phase diagram. Additionally, the design allows simultaneous measurement of transport properties.

II. PRESSURE CELL

The pressure-temperature phase diagram of interest for UGe_2 spans the region $T < 60$ K and $p < 1.6$ GPa.[13] This pressure range can be reached using a variety of cells, though the requirement for low temperatures precludes the use of large volume cells, such as the Paris-Edinburgh cell, or multi anvil devices.

Where the pulse echo technique is used, the length of the sample is an important parameter. If the path length for the ultrasonic pulse is too short, it can be challenging to disentangle pulses and echoes in the data. For that reason, it is preferable to choose the maximum possible sample length. Our cell had a total pressurised volume of 300 mm^3 with a maximum length of approximately 10 mm for the sample and the transducer.

A cross-section of the cell, modified from a design for high pressure neutron diffraction studies[14], is shown in Fig. 1. The body of the cell is made from BeCu, chosen for its high yield strength ($\sigma_y \approx 1.3$ GPa), and high thermal diffusivity over a broad temperature range, whilst remaining non-magnetic down to low temperatures ($\mu_r = 1.0018$).[15,16] The maximum operating pressure of the cell is 1.5 GPa, achieved through initially plastically deforming (autofrettaging) the cylinder, leaving the inner layer compressively supported by the surrounding elastic material of the cell.[17] The outer diameter of the cylinder is thinned to reduce the thermal mass, without compromising the strength of the cell.

[a)] Electronic mail: mkepa@staffmail.ed.ac.uk

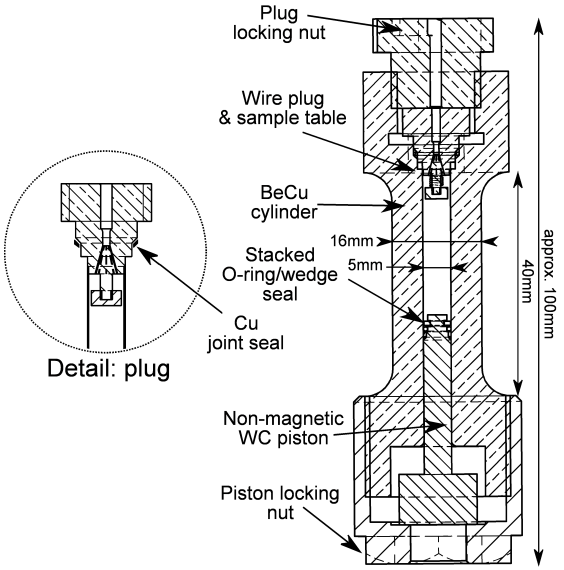

FIG. 1. Cross-sectional view of the pressure cell together with a detailed view of the plug. Description in the text.

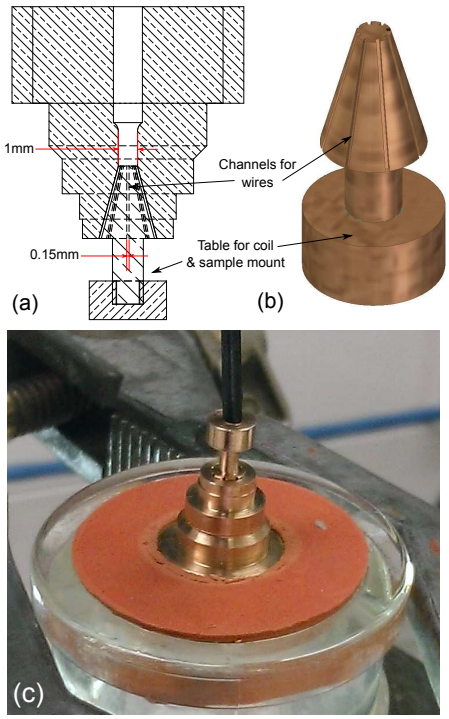

FIG. 2. (a) Cross-sectional view of the plug. (b) Rendered image of the plug with wire channels exposed. (c) Plug before application of Stycast (cone pointing down). The wires are fed through the channels, and a low suction-power pump is used to fill the remaining volume of the plug with Stycast.

The cell has been designed to include a wire feed-through plug (Fig. 2), carrying eight enamelled ø100 μm Cu wires to the sample region. This design incorporates a conical BeCu mandrel, or insert, which uses the 'unsupported area' principle to ensure that the pressure between the conical insert and the plug is always larger than the sample pressure, with epoxy sealing the space between the feed-through wires and the conical insert.[18] The design presented here uses narrow grooves to support the wires; a technique developed by J. Kamarád (Institute of Physics, Prague, Czech Republic).[19] This increases the length-to-diameter ratio for adhesive contact, making it less likely to leak, and more robust, reducing the possibility of the plug cutting the wires at high loads. Furthermore, the plug design allows a pin to be included to mount a manganin (CuMnNi alloy) sensor, and a table to precisely mount and align the sample. Four wires were used for four-terminal measurement of the resistivity of a manganin coil, used to determine the pressure in the cell over the full temperature range of operation.[20] Two were used for the transducer connection. Additional spare wires can potentially be used to perform simultaneous transport measurements or additional characterisation of the sample environment. The plug was sealed using Stycast 2850 FT with catalyst 23 LV. The manganin coil was wound and held using dilute GE varnish, and cycled under temperature and pressure to remove remnant hysteresis.

The sample is mounted on the table using an electrically insulating varnish (such as GE varnish). The electrical connections are then made by soldering, ensuring that they are properly insulated with varnish to prevent short circuits with the walls of the pressure cell. The plug is then inserted into the cell, and the locking nut tightened to deform the Cu wedge seal, Fig 1. The bore of the cell is filled through the piston end of the cell with a pressure medium (light mineral oil) avoiding air bubbles, leaving free space for the piston to initially engage with the bore. The piston has a two stage sealing mechanism: at low pressures the O-ring is sufficient to prevent any loss of pressure-transmitting medium; at higher pressures, the O-ring begins to extrude between the piston and the cylinder, deforming a Cu wedge seal. This design is beneficial, as no sample encapsulation is required, which otherwise reduces the available sample volume, and can interfere with wiring upon deformation. The two stage seal reduces friction at low pressures. This seal design required a profiled piston head which was initially machined from hardened BeCu. To reach the maximum pressure of the cell, this was replaced with a profiled WC piston.

The cell is loaded using a 5 tonne hydraulic press with a WC pusher, the piston is then locked in position using the locking nut. The resistivity of the manganin coil is continuously monitored allowing a precise pressure value to be measured. This is also used to check if the cell is sealed properly. Upon cooling it is common for pressure cells to lose a small amount of pressure due to thermal effects on the dimensions of the cell, and the behaviour of the pressure medium, though it is hard to predict what the drop in pressure will be; the manganin sensor re-

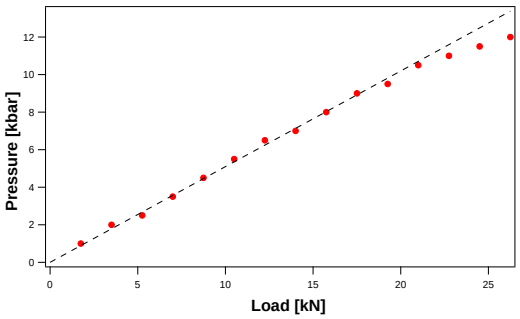

FIG. 3. The loading curve. The dotted line is the ideal pressure-load performance obtained from the force-area relation. The departure from linearity at 20 kN is most likely due to the deformation of the secondary Cu seal on the piston, which increases friction as compared with the O-ring.

moves this ambiguity. The loading curve of the cell is presented in Fig. 3. The loading mechanism allows for a fine pressure calibration in steps of 0.05 GPa.

FIG. 4. Loaded cell fixed to the cryostat holder.

The cell prepared for loading into the cryostat is presented in Fig. 4. A Cernox thermometer is mounted on the wall of the cell as close as possible to the position of the sample.

III. SAMPLE PREPARATION

The sample used in the experiment was a rectangular shaped single crystal of UGe_2 spark cut to the dimensions of 2.959×1.2×2 mm (length × height × width). Length (L) was measured (with a micrometer) to a greater precision than the other dimensions since it corresponded to the a-axis along which the ultrasound echoes were measured, Fig. 5(a). The orientation of the sample was determined by the back-reflection Laue x-ray method, scanning both top and bottom faces of the sample. The alignment was achieved to ±0.5°.

The pulse echo technique requires a fine surface finish but also adequate parallelism between the faces used in the measurement. Special care was taken when spark cutting the top and bottom faces of the sample. Afterwards, the sample was glued to a sapphire cylinder using commercially available crystal bond. The sapphire cylinder, machine-polished to high quality, was used to ensure parallelism of sample faces during polishing. The cylinder, with a sample mounted on top, was then inserted into the epoxy resin holder, Fig. 5(b). The void between the sample and the epoxy resin was filled in with wax in order to further support the sample during polishing, Fig. 5(b).

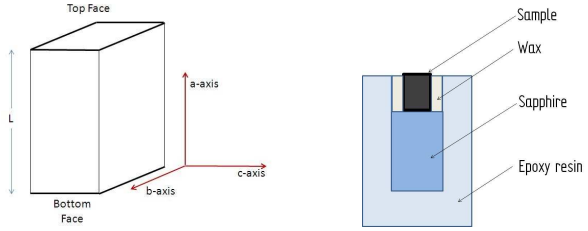

(a) (b)

FIG. 5. (a) Schematic figure of sample geometry. (b) Cross-sectional view of the sample holder prepared for the polishing process.

The process of manual polishing involved several steps, Fig. 6(a-c), with different grain sizes of silicon carbide grinding paper. The final stage of polishing was done on a soft polishing cloth with a diamond slurry with a grain size of 1 μm. The resulting average surface roughness was $\approx 1\,\mu$m, which was more than adequate since the ultrasound used in the experiment had a frequency of 50 MHz and speed of the order of 5000 ms^{-1}, and therefore a corresponding wavelength of 100 μm ($\gg 1\,\mu$m). The other side of the sample did not require such a fine finish and was polished with a diamond slurry with the grain size of 10 μm.

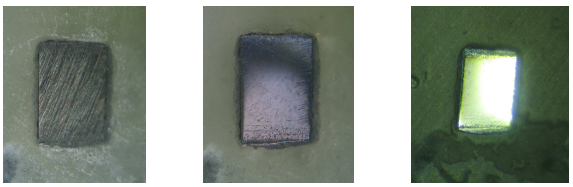

(a) (b) (c)

FIG. 6. Different stages of the sample polishing process. The pictures correspond to the following surface roughness: (a) 100 μm , (b) 10 μm and (c) 1 μm.

After the polishing process, the transducer was bonded to the smooth sample face. The transducer chosen was made from a commercially available material (from TRS Technologies, Inc.), TRS200HD, which belongs to the Lead Zirconate Titanate (PZT) type family. The transducer crystal was a 1 mm diameter disk with a fundamental frequency of 20 MHz with gold electrodes on the top and bottom of the crystal. The transducer was cut to produce longitudinal ultrasound, but due to its small size, excitation of other modes (transverse and/or quasi-transverse) also occurred. The transducer was bonded with cyanoacrylate − a clamp vice was used to ensure

good mechanical contact between the two elements and provide support during the setting of the adhesive.

The top face was used to mount the transducer, Fig. 7(a), the bottom was used to glue the sample to the pressure cell table, Fig. 7(b). Before loading the cell, the bonding was tested by measuring echoes at ambient temperature and pressure. An acceptable spectrum, such as one presented in the panel in Fig. 11, contained at least four echoes – otherwise the bonding process was repeated.

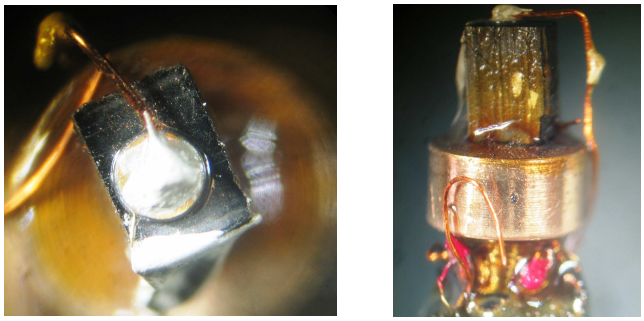

(a) (b)

FIG. 7. (a) Top-view: UGe_2 sample mounted on the pressure cell table with a piezoelectric crystal attached. (b) Side-view: the manganin coil is visible under the sample table.

IV. EXPERIMENTAL SETUP

The schematic diagram of the experimental setup is shown in Fig. 8. The loaded pressure cell was inserted into a closed cycle cryostat with a base temperature of 1.8 K. The transducer was connected to a wavegenerator, an amplifier and an oscilloscope, Fig. 8. The three pieces of the electronic equipment were:

1. DSOX6004A InfiniiVision Digital Storage Oscilloscope with sampling rate of 20 GS/s and 1GHz bandwidth.
2. DSOX6 WAVEGEN2 Dual Channel Wavegenerator with 200 MHz bandwidth.
3. A homemade Monolithic Amplifier with gain 10×.

The electronic block diagram of the setup is presented in Fig. 9(a). The transducer can be viewed as a capacitor which is connected in series with the wave generator and in parallel to the amplifier and oscilloscope. The schematic diagram of the amplifier with ± 5 V power supply is presented in Fig. 9(b). The amplifier is a non-inverting low noise op-amp with a gain of 10. A resistor of 50 Ω was added for impedance matching with the oscilloscope. The electronic setup does not allow lock-in type measurements, however it does offer robustness and simplicity in operation and also noise reduction due to the reduced number of electronic components in the circuitry.

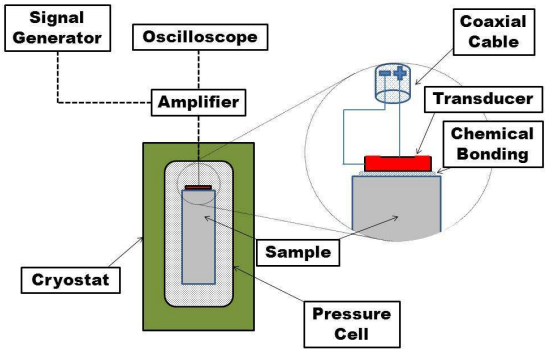

FIG. 8. Schematic figure of the experimental setup.

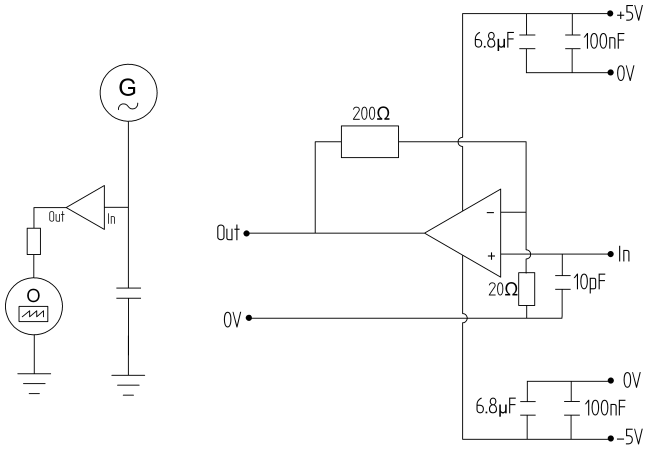

(a) (b)

FIG. 9. Block diagram of the of the experimental setup: **G** is the wave generator, **O** is the oscilloscope, the transducer is displayed as a capacitor. (b) Block diagram of the amplifier with a gain of 10.

V. DATA COLLECTION

All the results presented here were obtained using a single pulse mode and, hence, there was no need for a signal chopper in the circuitry. The initial half-sine pulse had a peak intensity of 2.5 V and a width of 10 ns corresponding to a band-width frequency of 100 MHz. The measurements were recorded with a LabView program which was controlling the oscilloscope settings but also the cooling rate and the temperature stability of the cryostat.

The measurements contained a spectrum of 8000 datapoints (x, y) each consisting of the values of voltage (y) and time (x). A average over 500 acquisitions of raw data was performed by the oscilloscope and recorded typically every 10 s. The temperature of the cryostat was ramped between 1.8-300 K at 0.1-0.5/min.

In order to identify the precise time location of the peak, and hence the speed of sound, we have used the

following function to fit the echoes in the spectrum

$$f(t) = \sin(\omega t + \phi)^* \left[f_{IC}(t - t_0)\right] \quad (1)$$

where f_{IC} is the Ikeda-Carpenter function[A] which was originally developed to describe the time evolution of a neutron peak travelling through a moderator.[21] In Eq. 1, ω is the sine frequency, ϕ is the phase shift and t_0 is the peak position. The function has a very steep rising exponential combined with a slower decaying exponential. An example of a fit to a peak (wavepacket) in the spectrum is presented in Fig. 10. The fitting function was used to identify the peak position and hence obtain the transit time given by $t_T = t_0 = \frac{2L}{v_L}$, i.e. the total time that it takes for the initial pulse to travel through the sample twice since the pulse is reflected by the back of the sample. The amplitude of the first peak was obtained from the raw data (without using the fit) using the maximum and the minimum value of the wavepacket. The obtained values of the transit time and the amplitude were then used to obtain the ultrasonic speed and attenuation coefficient as a function of temperature.

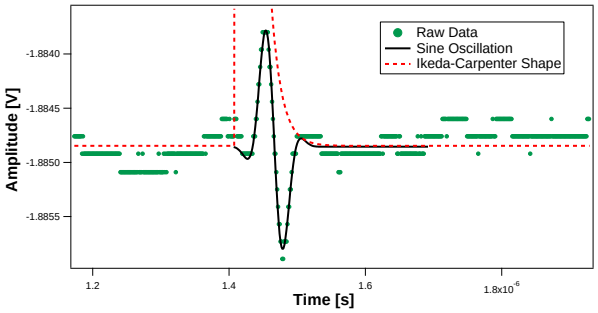

FIG. 10. Example of peak fitting. The red dashed curve is the Ikeda-Carpenter function describing the shape of the wavepacket envelope. The black solid curve is the oscillation term in the fitting function. Raw data is shown as green points.

VI. MEASUREMENTS ON UGe_2

In UGe_2, superconductivity is observed only in the ferromagnetic phase below 1 K in the pressure range between 0.8 and 1.6 GPa. The Curie temperature T_C and the transition line between paramagnetic and ferromagnetic (PM-FM) states are also fully suppressed at 1.6 GPa. The superconducting transition temperature is maximised, well inside the ferromagnetic phase, at $p_x = 1.2$ GPa which is also associated with a metamagnetic transition from the FM1 phase (lower moment/higher pressure) to FM2 phase (higher moment/lower pressure). It is believed that magnetic fluctuations associated with the FM1-FM2 transition might play a key role in the superconducting pairing mechanism.[22] The result presented here were obtained at a pressure of 1.1 GPa in the close vicinity of p_x. Previous elastic studies on UGe_2 were limited to ambient pressure.[23]

A. Elastic constant c_{11}

The elastic constant c_{11} was obtained from the relation

$$c_{11} = \rho v_L^2 \quad (2)$$

where ρ is the mass density and v_L is the longitudinal speed along the a-axis obtained from transit time t_0 discussed in the previous section. At room temperature and ambient pressure, the measured v_L was determined to be $4080 \pm 50\,\mathrm{ms}^{-1}$ which agrees well with the previous result obtained from neutron scattering.[24] The temperature evolution of c_{11} at 1.1 GPa is presented in Fig. 11. The high-temperature dependence is due to anharmonic phonon effects and can be viewed as a high temperature background. Elastic constant c_{11} exhibits two sharp peaks associated with two transition temperatures: T_x (FM1-FM2) and T_C (FM-PM).

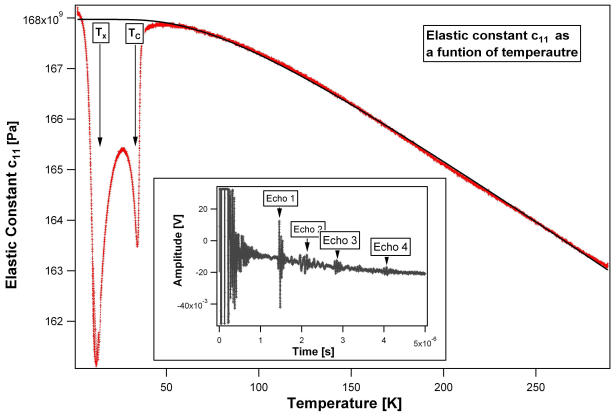

FIG. 11. Example of the pulse echo data taken at 1.1 GPa. The solid line is the high temperature fit. The inserted panel presents a raw spectrum of echoes at room temperature.

[A] Given by:
$f_{IC}(t-t_0) = \frac{\alpha^3}{2}\left\{(1-R)(t-t_0)^2 e^{-\alpha(t-t_0)} + \frac{2R\beta}{(\alpha-\beta)^3}\left[e^{-\beta(t-t_0)} - e^{-\alpha(t-t_0)}\left(\frac{(\alpha-\beta)^2(t-t_0)^2}{2} + (\alpha-\beta)(t-t_0)+1\right)\right]\right\}$
where α and β are exponential parameters (corresponding to fast and slow decays), R is the so-called mixing coefficient.[20]

The high temperature background could be modelled using[25]

$$c_{ij}(T) = c_{ij}^{o} - \frac{a}{e^{b/T} - 1} \tag{3}$$

with two free parameters a and b and zero temperature value c_{ij}^{o}. Parameter b can be associated with the Einstein temperature coming from the Einstein model and the value obtained from the fit was 224±1 K. The value of c_{ij}^{o} was 167.97±0.02 GPa and a was 5.79±0.02 GPa. Both transitions are magnetic in origin suggesting strong electron-phonon coupling i.e. a strong magnetoelastic effect.

B. Ultrasonic Attenuation

The ultrasonic attenuation coefficient is defined as $\alpha = 20\frac{1}{x_2 - x_1}\log\left(\frac{A(x_1)}{A(x_2)}\right)$, where $A(x_1)$ and $A(x_2)$ are the amplitudes of the ultrasonic wave at positions x_1 and x_2. Here, we present a relative change of the attenuation coefficient as a function of temperature such that

$$\alpha_{relative} \propto \ln\left(\frac{A(T)}{A_0}\right) \tag{4}$$

where A_0 is the amplitude of the first echo at room temperature and $A(T)$ is its value at any given temperature. The temperature evolution of the relative attenuation coefficient is presented in Fig. 12. Both transition temperatures can be easily identified. The ultrasonic attenuation coefficient can be shown to be proportional to the space-time Fourier-Laplace transform of a four-spin correlation function.[26] However, a full interpretation of these observations requires further studies at different driving frequencies since the value of the attenuation is a frequency dependent quantity.

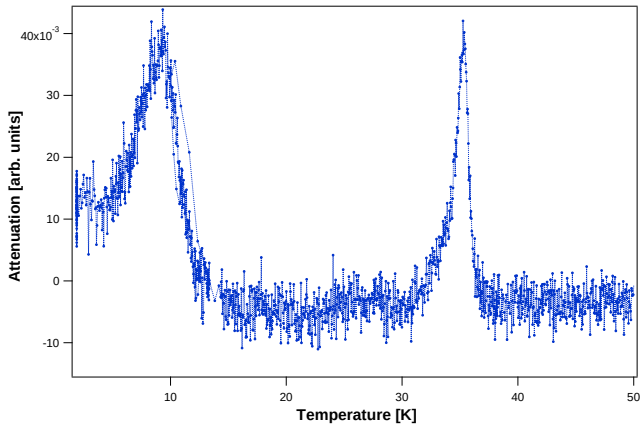

FIG. 12. Relative change of the attenuation coefficient as defined in the text obtained at 1.1 GPa.

VII. CONCLUSIONS

In conclusions, we have presented a fully functional piston cylinder cell for making pulse echo measurements. The main advantages of the setup are as follows: a simple electronic setup with few elements (single coaxial cable, oscilloscope, wave generator and amplifier), accurate pressure control and an ability to measure transport measurements simultaneously with ultrasonic quantities as well as *in situ* pressure calibration. Introduction of the transducer inside the pressure space reduces the background and simplifies data analysis. The measurement sensitivity achieved in the setup detected relative changes of the elastic constant of 4×10^{-4}.

The work can be extended to measure ultrasonic pulses at different frequencies, lower temperatures and also in high magnetic fields.

ACKNOWLEDGMENTS

We acknowledge EPSRC for providing the financial support (Grant No EP/J00099X/1). We thank Jim Stuart (School of Physics and Astronomy, University of Edinburgh) for setting up the electronics and Dave McCabe (Engineering Workshop, University of Edinburgh) for technical support.

[1] B. Luthi, in *Physical Acoustics in the Solid State* (Springer, 2005) Chap. 4.
[2] R. Truell, *Ultrasonic methods in solid state physics* (New York, 1969).
[3] M. Gauthier, D. Lheureux, F. Decremps, M. Fischer, J. P. Itié, G. Syfosse, and A. Polian, Review of Scientific Instruments **74**, 3712 (2003).
[4] S. D. Jacobsen, H. J. Reichmann, A. Kantor, and H. A. Spetzler, Advances in High-Pressure Techniques for Geophysical Applications **2**, 25 (2005).
[5] O. F. Yagafarov, E. L. Gromnitskaya, A. G. Lyapin, and V. V. Brazhkin, Journal of Physics: Conference Series **215**, 012054 (2010).
[6] H. J. Mueller, J. Lauterjung, F. R. Schilling, C. Lathe, and G. Nover, European Journal of Mineralogy **14**, 581 (2002).
[7] K. L. Darling, G. D. Gwanmesia, J. Kung, B. Li, and R. C. Liebermann, Physics of the Earth and Planetary Interiors **143**, 19 (2004).
[8] S. D. Jacobsen, H. Spetzler, H. J. Reichmann, and J. R. Smyth, Proceedings of the National Academy of Sciences of the United States of America **101**, 5867 (2004).
[9] S. Adenwalla, S. W. Lin, Z. Zhao, J. B. Ketterson, J. A. Sauls, D. G. Hinks, M. Levy, and B. K. Sarma, Physical Review Letters **65**, 2298 (1990).
[10] B. Ellman, L. Taillefer, and M. Poirier, Physical Review B **54**, 9043 (1996).
[11] M. Boukhny, G. L. Bullock, B. S. Shivaram, and D. G. Hinks, Physical Review Letters **73**, 1707 (1994).
[12] T. Yanagisawa, Philosophical Magazine **94**, 3775 (2014).
[13] S. Saxena, P. Agarwal, K. Ahilan, F. Grosche, R. Haselwimmer, M. Steiner, E. Pugh, I. Walker, S. Julian, P. Monthoux, G. Lonzarich, A. Huxley, I. Sheikin, D. Braithwaite, and J. Flouquet, Nature **406**, 587 (2000).
[14] W. Wang, D. A. Sokolov, A. D. Huxley, and K. V. Kamenev, Review of Scientific Instruments **82**, 073903 (2011).
[15] B. A. Jordan, Journal of Materials Science **4**, 1097 (1969).

[16] J. Ekin, in *Experimental Techniques for Low-Temperature Measurements* (Oxford University Press, 2006).
[17] D. S. Tsiklis and T. Scott, Physics Today **23**, 68 (1970).
[18] M. I. Eremets, *High Pressure Experimental Methods* (Oxford University Press, 1996).
[19] J. Kamarád, *private communication* (2015).
[20] L. H. Dmowski and E. Litwin-Staszewska, Measurement Science and Technology **10**, 343 (1999).
[21] S. Ikeda and J. M. Carpenter, Nuclear Instruments and Methods in Physics Research **239**, 536 (1985).
[22] A. Huxley, Physica C: Superconductivity and its Applications **514**, 368 (2015).
[23] K. Kuwahara, T. Sakai, M. Kohgi, Y. Haga, and Y. Onuki, Journal of Magnetism and Magnetic Materials **310**, 362 (2007).
[24] S. Raymond and A. Huxley, Physical Review B **73**, 094420 (2006).
[25] Y. Varshni, Physical Review B **2**, 3952 (1970).
[26] B. Luthi, in *Physical Acoustics in the Solid State* (Springer, Berlin, 2005) Chap. 6, pp. 93–108.